Direct Reading of the Nonlinear Optical Response via Spatial Mapping

Pengbo Jia,[1,§] Domenico Bongiovanni,[1,2,§] Yi Hu,[1,*] Roberto Morandotti,[2,3] Zhigang Chen,[1,4,†] and Jingjun Xu[1,‡]

[1] *The MOE Key Laboratory of Weak-Light Nonlinear Photonics, TEDA Applied Physics Institute and School of Physics, Nankai University, Tianjin 300457, China*

[2] *INRS-EMT, 1650 Blvd. Lionel-Boulet, Varennes, Quebec J3X 1S2, Canada*

[3] *Institute of Fundamental and Frontier Sciences, University of Electronic Science and Technology of China, Chengdu 610054, China*

[4] *Department of Physics and Astronomy, San Francisco State University, San Francisco, California 94132, USA*

(Received 29 September 2020; revised 25 October 2020; accepted 26 October 2020; published 1 December 2020)

We propose and demonstrate a scheme for spatial mapping and direct reading of the nonlinear response of optical materials from the propagation of self-accelerating beam profiles. Through a single evolution measurement, a two-dimensional compact Airy beam is able to directly map the nonlinear response of a medium into spatial profiles. The most efficient mapping takes place along some particular transverse directions rather than the direction of the beam acceleration, depending on both the Airy intensity pattern and the type of nonlinearity. Our work may herald a simple yet effective way for measuring the nonlinear optical response, in contrast to the conventional *Z*-scan technique.

DOI: 10.1103/PhysRevApplied.14.064001

I. INTRODUCTION

Measuring the nonlinear optical response of a medium is relevant in both fundamental studies and various technological applications. Knowing the response function not only offers crucial information for analyzing or designing the properties of nonlinear media but would also allow mathematical models to be built to uncover complex nonlinear behaviors and guide relevant experimental studies. In general, to estimate the nonlinear response as a function of the light intensity, the study of multiple nonlinear evolutions is typically required, as routinely done in the well-known *Z*-scan method [1,2]. Consequently, the resulting data collection and subsequent analysis are time consuming, and in some cases, multiple measurements can lead to an increased complexity of the experimental setup [3].

Recently, it was found that a nonlinear-response function can be spatially mapped directly onto a nonlinearity-shaped beam profile [4]. The mapping was realized by propagating a structured optical field, namely an Airy beam [5], in the presence of nonlinearity. The main mechanism affecting the beam-profile evolution is the gravitylike potential brought by the self-acceleration inherent to Airy-like waves [6]. This simple process offers possibilities to reduce the complexity typically involved in conventional nonlinear-response measurements. Although very promising, spatial mapping has only been demonstrated in a one-dimensional (1D) configuration, thus limiting potential applications. Indeed, a 1D Airy beam occupies a large amount of space as it greatly extends along one transverse direction, thus leading to difficulties if the nonlinear medium under test has a small size. Besides, the limited light confinement results in a large energy spreading that hampers the ability to reach high intensities. Consequently, more power has to be consumed to induce the strong nonlinearity necessary for high-fidelity mapping. To overcome these disadvantages, new approaches exploiting more confined probe beams should be developed and explored to make this technique more practical and appealing.

In this work, we propose and demonstrate a scheme to employ compact self-accelerating optical beams to probe nonlinear media. Relying on the accelerating property of a two-dimensional (2D) Airy beam, the nonlinear response of a medium can be spatially mapped in various transverse directions. It is found that the high fidelity of the mapping (i.e., the ability to properly reproduce the nonlinear response) occurs along the directions defined by the peak intensity and skewed with respect to the overall beam acceleration. The orientations that lead to the optimal mapping are influenced by both the Airy-beam pattern and the nonlinear-response function. Our method may lead to an efficient way of examining the nonlinear medium response.

*yihu@nankai.edu.cn
†zgchen@nankai.edu.cn
‡jjxu@nankai.edu.cn
§These authors contribute equally to this work.

II. THEORETICAL AND NUMERICAL ANALYSIS

In the nonlinear regime, the dynamics of a laser beam is generally governed by a paraxial wave equation, namely the generalized nonlinear Schrödinger equation, given as [7]

$$\frac{\partial\psi}{\partial z}-\frac{i}{2k}\left(\frac{\partial^2\psi}{\partial x^2}+\frac{\partial^2\psi}{\partial y^2}\right)+if\,(I)\,\psi=0, \qquad (1)$$

where $\psi(x,y,z)$ represents the electric field amplitude of the optical beam, x and y are the transverse coordinates, z is the propagation distance, k is the wave number, $f\,(I)$ is a real-valued algebraic function that accounts for a nonlinear response, and $I=|\psi|^2$ denotes the light intensity. Here, only self-defocusing nonlinearities are considered, since equivalent dynamics with self-focusing nonlinearity can be studied, e.g., by employing diffraction management brought by periodic structures [8]. In a moving reference frame [9–11] defined by $s_x=(x-y)/\sqrt{2}-g(z)$ and $s_y=(x+y)/\sqrt{2}-g(z)$ [where $g(z)$ represents the moving path], Eq. (1) can be reformulated as

$$\frac{\partial\psi}{\partial z}-\frac{dg}{dz}\left(\frac{\partial\psi}{\partial s_x}+\frac{\partial\psi}{\partial s_y}\right)-\frac{i}{2k}\left(\frac{\partial^2\psi}{\partial {s_x}^2}+\frac{\partial^2\psi}{\partial {s_y}^2}\right)+if\,(I)\,\psi=0. \qquad (2)$$

In the specific frame, i.e., where $g(z)=hz^2/2$ (h is a constant), the dynamics governed by the above equation becomes stationary by letting $\psi(x,y,z)=u(s_x,s_y)\exp[i\sqrt{2}hxz+ih^2z^3/(3k)]$:

$$\frac{1}{2k}\left(\frac{\partial^2u}{\partial {s_x}^2}+\frac{\partial^2u}{\partial {s_y}^2}\right)-\sqrt{2}hxu-f\,(I)u=0. \qquad (3)$$

Assuming that the propagation environment is a strong self-defocusing regime, the beam tends to have a broad size. As such, the diffraction term in Eq. (3) can be neglected under the Thomas-Fermi approximation [12]. Consequently, the nonlinear response can be directly mapped onto the abscissa through

$$x=-f\,(I)/(\sqrt{2}h). \qquad (4)$$

In other words, it is possible to read out the nonlinear-response function directly in the intensity profile of a nonlinearly-shaped light. For this mapping, the linear gravitylike potential expressed as $\sqrt{2}hx$ in Eq. (3) plays a crucial role. It is worth noting that such a potential is not applied externally, but it is associated with the diffraction in the chosen accelerating frame. In order to verify the analysis, numerical simulations are performed for the specific case of a Kerr nonlinearity [i.e., $f\,(I)=n_2I$]. Without loss of generality, we assume that the nonlinear coefficient n_2 takes a value of -1.6×10^{-5} cm^2/W [13]. The gravitylike effect is introduced through the self-acceleration of a 2D Airy beam, a solution to Eq. (3) in the absence of the nonlinear term. Before performing the nonlinear test, the peak intensity of the Airy beam is intentionally delivered to the output in a linear propagation regime [4]. Under this condition, the light intensity in the early stage is kept at a quite low level during the nonlinear evolution, allowing a well-maintained beam acceleration as if there is a gravitylike potential. For this purpose, a quadratic phase expressed as $\exp[ib({k_x}^2+{k_y}^2)]$ is imparted to the Airy beam in the momentum space (defined by k_x and k_y). The parameter b is used to alter the longitudinal location of the peak intensity. Figures 1(a1)–1(a3) illustrate the nonlinear evolution of a 2D Airy beam in a 10-mm-long Kerr medium. As expected, the intrinsic acceleration (predesigned along the x direction) is well sustained [Fig. 1(a1)]. At the output, the beam exhibits significant broadening when compared to the linear case, particularly for the main lobe that experiences the strongest nonlinearity [Figs. 1(a2) and 1(a3)]. To corroborate the theory above, the light profile extracted from the nonlinear output pattern along the x axis is examined. Obviously, the right side of the profile is nonlinearly shaped into a tilted straight line [Fig. 1(a3)], in qualitative accordance with the spatial mapping (i.e., $I\propto x$) built using Eq. (4) for a third-order nonlinear optical Kerr response.

In the following, we show the need of beam acceleration for this mapping. In the Cartesian coordinates rather than in the accelerating frame, Eq. (1) becomes stationary by using the substitution $\psi(x,y,z)=\varphi(x,y)\exp(i\delta z)$ [14,15]:

$$\frac{1}{2k}\left(\frac{\partial^2\varphi}{\partial x^2}+\frac{\partial^2\varphi}{\partial y^2}\right)-\delta\varphi-f\,(I)\varphi=0, \qquad (5)$$

where δ is a propagation constant. Neglecting the diffraction term as done in the accelerating case, the above formula reduces to $f\,(I)=-\delta$, indicating a possible flat intensity distribution in an optical wave experiencing a self-defocusing nonlinearity. This intensity feature is independent of the nonlinear form, and in turn, it cannot display a nonlinear response. As an illustrative example, the same Kerr nonlinearity is probed numerically by a nonaccelerating beam (here we assume a common Gaussian beam) [Figs. 1(b1)–1(b3)]. Similar to the Airy case, the Gaussian waist is set to appear at the output in the linear propagation. Under the action of the nonlinearity, the beam further expands uniformly towards all radial directions and forms a flat-top feature at the output [16–18]. By further examining the edges of the intensity profile [Fig. 1(b3)], there is no evident straight-line distribution characterizing the spatial mapping of the Kerr nonlinear response. In particular, the beam edges tend to undergo a progressive steepening under a strong defocusing nonlinearity and, eventually, they develop into a gradient catastrophe

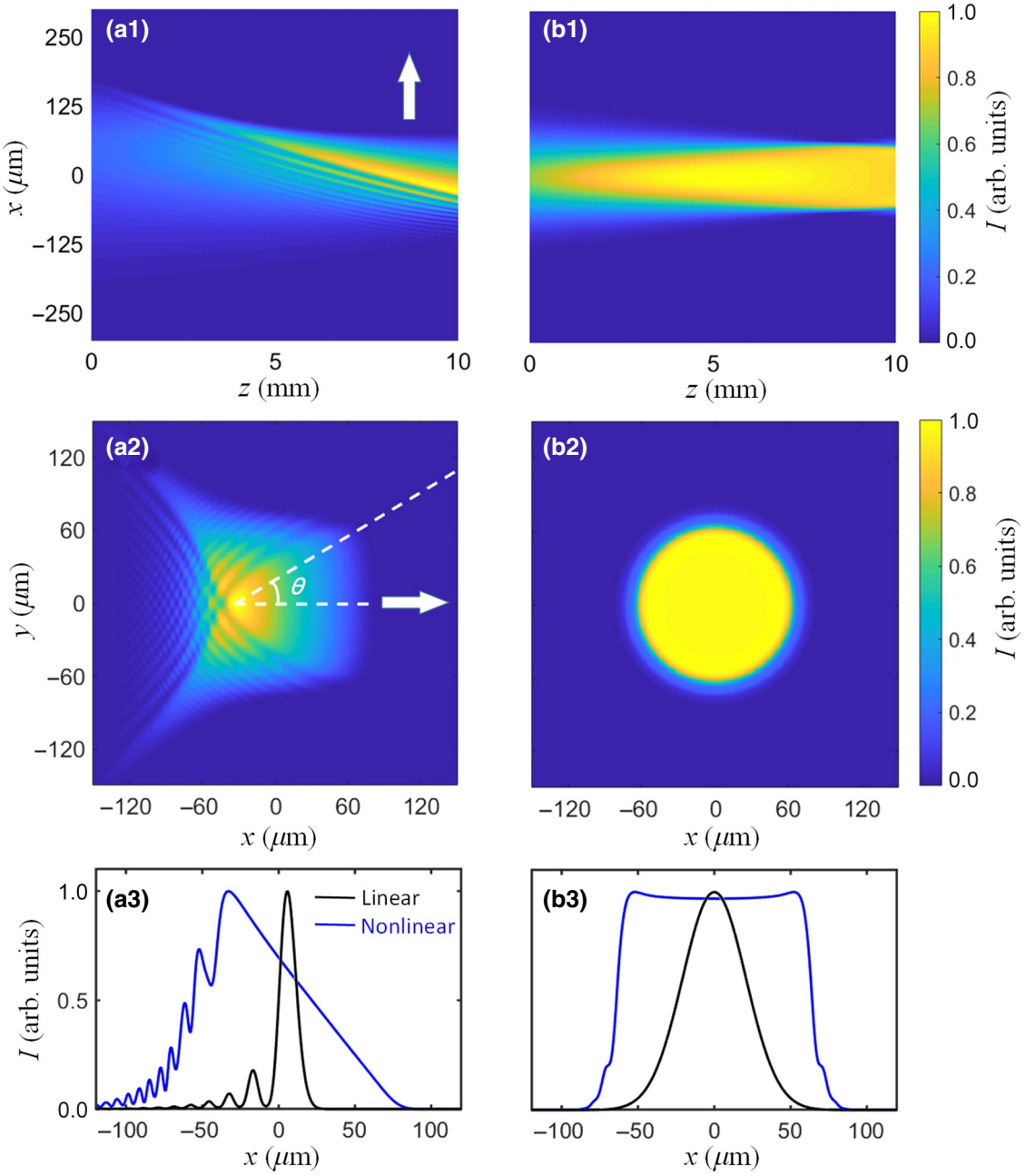

FIG. 1. Numerical evolutions of a 2D Airy beam (left column) and a Gaussian beam (right column) in a Kerr medium. Upper panels illustrate the normalized longitudinal intensity distributions. Middle panels correspond to the transverse beam patterns at the output. Bottom panels compare the normalized linear and nonlinear output intensity profiles along the x axis. Arrows in (a1) and (a2) point to the acceleration direction of the Airy beam.

(or shock-wave formation) [19]. The resulting dispersive shock wave mixes nonlinear and diffractive effects, thus preventing the spatial mapping [19–21]. Therefore, the beam acceleration, as illustrated here by the specific Airy field, is necessary to spatially map the nonlinear response.

Considering that the acceleration in a 2D configuration has a vectorial nature, the spatial mapping may exist even along other directions, rather than only along the x axis. This is also supported by the fact that the linear potential required for the mapping is indeed present in any direction as inferred from Eq. (3). In particular, along an arbitrary line given by $y = tg(\theta)x + c$ [where c is a constant, and θ is the angle defined in Fig. 1(a2), i.e., the direction is given with respect to the beam-acceleration direction], the linear potential goes as $\sqrt{2}hx\cos\theta$. To examine the possibility of multidirectional mapping, the beam

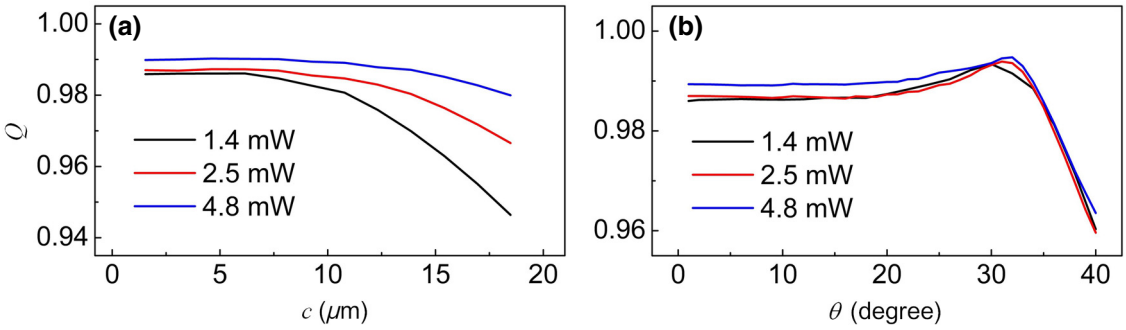

FIG. 2. Multidirectional spatial mapping of the Kerr nonlinear response via the nonlinear evolution of a 2D Airy beam. Calculated fitting coefficient Q along horizontal (a) and radial (b) directions in the output Airy patterns, parameterized with different input powers.

profiles in the Airy output patterns are extracted along different orientations. In order to characterize the mapping quality, we define $Q = 1 - \sqrt{\sum (D - I)^2 / \sum D^2}$, where D includes the fitting data generated via Eq. (4). Q ranges from 0 to 1, with a larger value corresponding to a stronger similarity (i.e., a higher mapping fidelity) between a target light profile and the nonlinear response. Specifically, to fit the target curves, we employ four fitting parameters d_1, d_2, d_3, and d_4 to linearly reshape Eq. (4) as $(x-d_1)/d_2 = f[(I-d_3)/d_4]$. The optimal values of these fitting parameters are obtained by means of the MATLAB tool "nlinfit." Then the fitting curve D can be calculated through $D = f^{-1}[(x-d_1)/d_2] \times d_4 + d_3$, where f^{-1} is the inverse function of the nonlinear-response function. First, we consider directions parallel to the x axis (i.e., $\theta = 0$). The linear trend associated with the Kerr response is still observed in the right sides of the y-cut profiles. The calculated value of Q shows a deterioration of the mapping quality as the y-cut profile moves away from $y = 0$ [Fig. 2(a)]. Along these directions parallel to the x axis, since the associated linear potentials are identical (i.e., $\sqrt{2}hx$), a better mapping is expected in a stronger nonlinear regime (corresponding to a higher peak intensity), beneficial to neglect diffraction more safely. In particular, different Q values associated with disparate y-cut profiles show only a small divergence for large input powers, as they tend to approach the upper limit. Second, the beam profiles are extracted along radial directions (i.e., $\theta \neq 0$) fixed to the peak intensity for pursuing the strongest nonlinear regime in each direction. Considering the symmetry of the 2D Airy beam with respect to the x axis, only the cases of positive angles are discussed, as shown in Fig. 2(b). As θ increases, the mapping initially experiences a nearly invariant change and subsequently improves until reaching the best condition at around $\theta = 30°$, after which a fast drop of the fidelity occurs. Apparently, the mapping is optimal in a direction significantly skewed with respect to the x axis which is defined as the overall acceleration direction of the 2D Airy beam. This outcome is reasonable by reconsidering the role played by the linear potential. A smaller steepness of the potential corresponds to a larger beam expansion and accordingly, a decrease in the diffraction impact. Thus the value of Q is expected to increase as θ becomes large. However, this rule fails to apply for quite large angles, as the sublobes of the Airy beam alter the linear shape of the potential. Consequently, the optimal angle is determined by both the acceleration direction and the structure of the 2D Airy beam. Even when more power is injected, the optimal angle only exhibits a slight increase, indicating the stability of the beam structure under a strong nonlinearity.

III. EXPERIMENTAL METHODS AND RESULTS

In our experiment, we demonstrate the above analyzed spatial mapping in a 10-mm-long strontium-barium niobate photorefractive (PR) crystal. A self-defocusing nonlinearity is readily activated by externally applying a bias field parallel to the crystalline axis [22]. The associated nonlinear response is formulated as $f(I) = -0.5 n_0^3 \gamma_{33} E_e/(1 + I)$, where $n_0 = 2.3$ is the refractive index of the crystal, $\gamma_{33} = 280$ pm/V is the electro-optic coefficient for extraordinarily polarized light, and E_e is the bias field. Figure 3(a) illustrates a schematic setup. A standard technique [5] is used to produce 2D Airy beams, based on Fourier transforming an expanded laser beam (from a cw laser operating at $\lambda = 532$ nm) featuring a Gaussian-like profile (the waist being $w_0 = 2$ mm) together with proper phase modulations applied by a phase-only spatial light modulator (SLM). In order to position the peak intensity of the Airy beams at the output, the exiting facet of the PR crystal is overlapped with the focal plane of the lens performing the Fourier transform. The probe beam power is intentionally fixed at 19.5 μW, a value far below the saturation level of the PR nonlinearity, while the nonlinear strength is tuned by adjusting the bias field. The intensity patterns at the output are recorded by an imaging system consisting of a spherical lens and a CCD camera. Experimental results obtained under different bias fields are presented in Figs. 3(b1)–3(b3). The main lobe of the

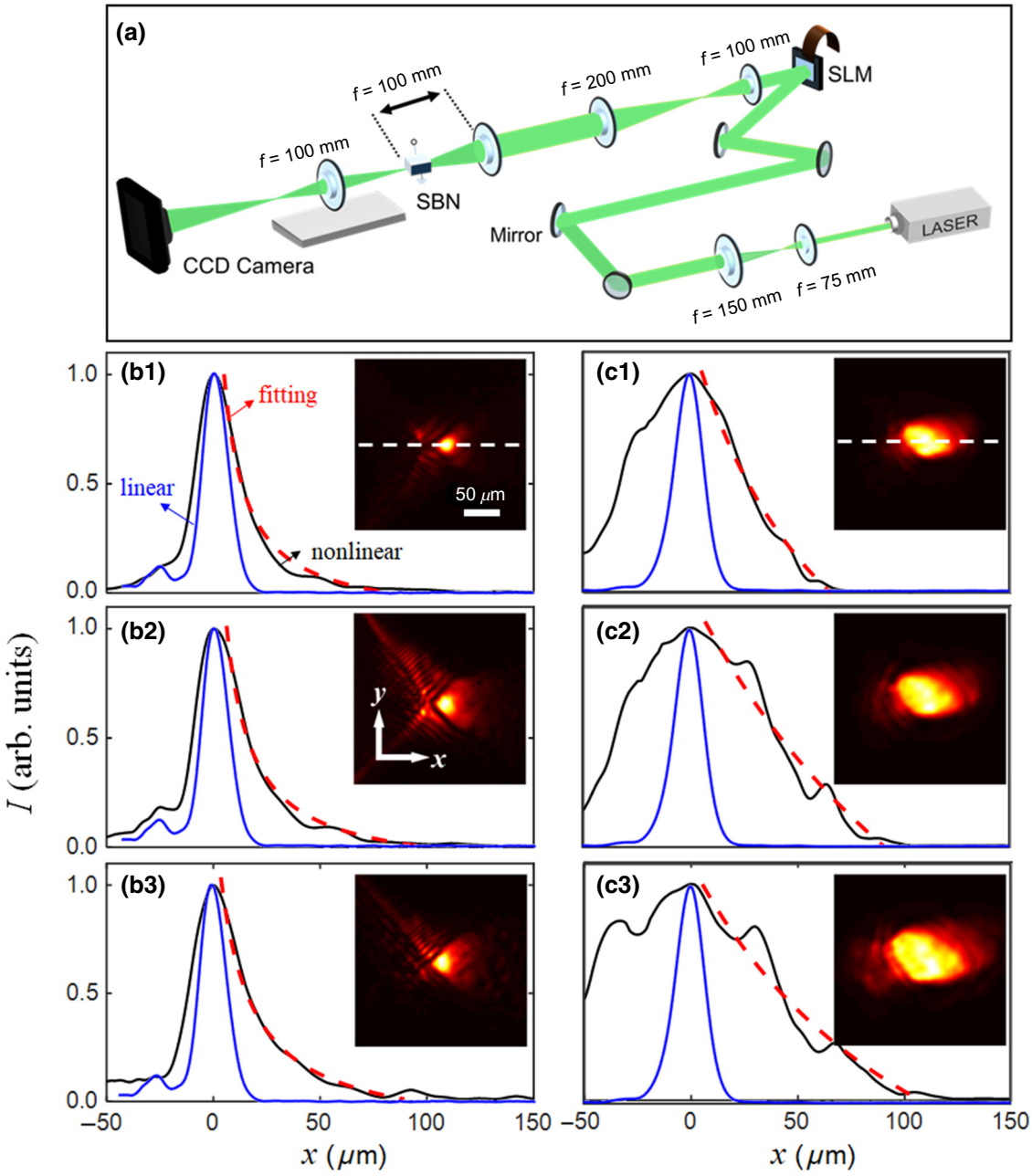

FIG. 3. (a) Schematic setup. (b1)–(b3), (c1)–(c3) Experimentally observed nonlinear output patterns (insets) for a 2D Airy beam (b1)–(b3) and a Gaussian-like beam (c1)–(c3) propagating in the PR crystal with different bias fields (from the first to the third rows: $E_e = -110$, -150, and -170 kV/m). Blue and black solid curves are intensity profiles extracted from linear and corresponding nonlinear outputs along the x axis (white dashed line), respectively. The red dashed curves, calculated from Eq. (4), are used for fitting the right edge of each profile.

Airy beam clearly expands as the nonlinearity is strengthened, allowing for the possibility to isolate the nonlinear effect from normal diffraction. To examine the output in more detail, the beam profile along the x axis (coinciding with the overall beam acceleration) is selected. In contrast to the overall expansion for the Kerr case, the beam broadening mainly occurs at the lower intensity part of the right edge. Indeed, as a result of the acceleration, this right side tends to be reshaped into a profile described by the inverse linear response function typical of a PR nonlinearity. It can be properly fitted by using Eq. (4), especially for strong nonlinearities, thus evidencing the spatial mapping of the PR nonlinear response. For a direct comparison, a Gaussian-like beam is also used for probing the nonlinear crystal. To this end, the imposed phase pattern for generating the Airy beam is switched off on the SLM. In this

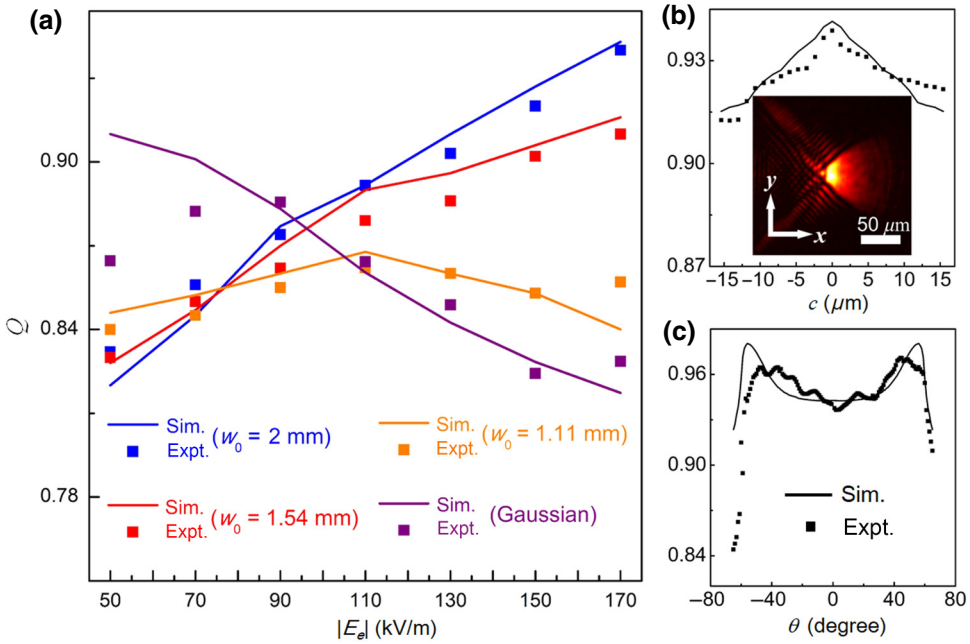

FIG. 4. Multidirectional spatial mapping of the PR nonlinear response at the output of nonlinear evolutions associated to a 2D Airy beam. (a) Calculated fitting coefficient Q versus the bias field for different input conditions. (b), (c) Q values along horizontal (b) and radial (c) directions of the nonlinear output pattern shown in the inset of (b).

way, the associated beam waist appears at the exiting facet of the crystal after linear propagation. Under the action of the nonlinearity, the output experiences a radial expansion. The beam profiles along the x axis are further extracted for clarity. Unlike the obvious asymmetric broadening for the Airy case, the Gaussian-like beam undergoes an expansion occurring in both sides [Figs. 3(c1)–3(c3)]. As the nonlinearity increases, more power flows outside. The resulting less-dominated intensity near the center is consistent with the theoretical prediction of an intensity plateau. The ideal flat-top feature is not observed in our measurements due to an imperfect quality of the laser mode. For a low bias field (i.e., $E_e = -110$ kV/m), the right side of the extracted profile fits the PR response function. Nevertheless, it is observed that the fitting gets worse as the nonlinearity is turned up, since a shock-wave formation takes place, thus preventing the isolation of the nonlinear effect from diffraction. In this sense, the spatial mapping of the nonlinear response cannot work for a Gaussian-like beam. To characterize the mapping quality, we further calculate the Q coefficients. Blue and purple squares correspond to the Airy and Gaussian cases in Fig. 4, respectively. Clearly, Q becomes larger as the nonlinearity is strengthened for the Airy case. In contrast, it cannot reach a high value for the Gaussian case, but it rather shows a decay for stronger nonlinearities. Furthermore, the effect of shortening the Airy sublobes (necessary for beam acceleration) is discussed. The associated apodization is readily realized by reducing the waist of the beam illuminating the SLM via an iris [5]. As long as a sufficient number of sublobes are kept to induce the acceleration, the spatial mapping can still be realized. For instance, when w_0 is reduced to 1.54 mm, Q increases with the bias field. The growth rate becomes slow upon the use of an apodization, as the resulting power loss exerts a negative impact on the nonlinear strength. A relatively larger apodization (say $w_0 = 1.1$ mm) leads to an increase of Q only with a mild bias field. In these nonlinear conditions, one can infer that the beam acceleration persists. However, we note that for stronger nonlinearities, the acceleration tends to disappear, since Airy beams with a small number of sublobes cannot persist when propagating in a highly nonlinear regime. Consequently, for $|E_e| > 110$ kV/m, the value of Q experiences a drop, showing once again the relevance of using acceleration for realizing the spatial mapping.

Finally, we turn our attention to examine the Q coefficient along other transverse directions. In order to guarantee a vertically symmetric beam profile under a strong nonlinearity, the measurement is performed by involving more sublobes in the Airy beam, which can be easily achieved through slightly shifting the PR crystal backward relative to the beam propagation direction. The other conditions are kept the same as those in Fig. 3(b3). Clearly, the nonlinear output pattern [see the inset in Fig. 4(b)] has an improved symmetry as compared to that in the inset of Fig. 3(b3). By setting the origin point at the location of the peak intensity, the beam profiles along different directions are then extracted. As shown in Figs. 4(b) and 4(c), the mapping features are similar to those for the Kerr case: for horizontal directions, the value of Q experiences a continuous decrease as the beam profile is extracted away from $y = 0$; while for skewed directions, the maximum value of Q appears at a certain angle. For the PR case, the optimal angle exhibits a much larger value than the Kerr case, as also confirmed by our numerical simulations. By comparing the main lobes in the two cases,

we notice significantly different shapes. Under a PR nonlinearity, the beam expansion appears at wider angles, leading to a larger optimal skewing because of a more extended range where beam sublobes have no influence. In this regard, the ideal angle is determined not only by the acceleration and structure of the Airy beam, but it also depends on the type of the nonlinear response under test.

IV. CONCLUSION

In conclusion, we demonstrate a scheme for multidirectional spatial mapping of the material's nonlinear optical response by using a 2D Airy beam. We test both Kerr and PR nonlinearities and find that the optimal mapping for efficient reading of the nonlinear response appears along a particular radial direction, forming an angle with respect to the beam acceleration direction. Such a direction is influenced by the Airy-beam structure as well as the type of nonlinear response. Our results may lead to a direct visualization of the nonlinear response in a more accessible way.

ACKNOWLEDGMENTS

We acknowledge financial support from National Key R&D Program of China (Grant No. 2017YFA0303800), National Natural Science Foundation of China (12022404, 62075105, 91750204), the NSERC Discovery and Canada Research Chair Grants in Canada, and the MEI in Quebec. D.B. acknowledges support from a China Postdoctoral Science Grant (66 Call). R.M. is affiliated to UESTC as an adjoining faculty.

[1] R. L. Sutherland, *Handbook of Nonlinear Optics* (CRC Press, New York, 2003).
[2] M. Sheik-Bahae, A. A. Said, and E. W. Van Stryland, High-sensitivity, single-beam n_2 measurements, Opt. Lett. **14**, 955 (1979).
[3] G. Boudebs, M. Chis, and X. Nguyen Phu, Third-order susceptibility measurement by a new Mach–Zehnder interferometry technique, J. Opt. Soc. Am. B **18**, 623 (2001).
[4] P. Jia, Z. Li, Y. Hu, Z. Chen, and J. Xu, Visualizing a Nonlinear Response in a Schrödinger Wave, Phys. Rev. Lett. **123**, 234101 (2019).
[5] G. A. Siviloglou, J. Broky, A. Dogariu, and D. N. Christodoulides, Observation of Accelerating Airy Beams, Phys. Rev. Lett. **99**, 213901 (2007).
[6] N. K. Efremidis, Z. Chen, M. Segev, and D. N. Christodoulides, Airy beams and accelerating waves: An overview of recent advances, Optica **6**, 686 (2019).
[7] Y. S. Kivshar, and G. P. Agrawal, *Optical Solitons: From Fibers to Photonic Crystals* (Academic Press, New York, 2003).
[8] H. S. Eisenberg, Y. Silberberg, R. Morandotti, A. R. Boyd, and J. S. Aitchison, Discrete Spatial Optical Solitons in Waveguide Arrays, Phys. Rev. Lett. **81**, 3383 (1998).
[9] I. Kaminer, M. Segev, and D. N. Christodoulides, Self-accelerating Self-Trapped Optical Beams, Phys. Rev. Lett. **106**, 213903 (2011).
[10] A. Lotti, D. Faccio, A. Couairon, D. G. Papazoglou, P. Panagiotopoulos, D. Abdollahpour, and S. Tzortzakis, Stationary nonlinear Airy beams, Phys. Rev. A **84**, 021807(R) (2011).
[11] Y. Hu, Z. Sun, D. Bongiovanni, D. Song, C. Lou, J. Xu, Z. Chen, and R. Morandotti, Reshaping the trajectory and spectrum of nonlinear airy beams, Opt. Lett. **37**, 3201 (2012).
[12] L. V. Hau, B. D. Busch, C. Liu, Z. Dutton, M. M. Burns, and J. A. Golovchenko, Near-resonant spatial images of confined Bose-Einstein condensates in a 4-Dee magnetic bottle, Phys. Rev. A **58**, R54(R) (1998).
[13] V. Smith, B. Leung, P. Cala, Z. Chen, and W. Man, Giant tunable self-defocusing nonlinearity and dark soliton attraction observed in m-cresol/nylon thermal solutions, Opt. Mater. Express **4**, 1807 (2014).
[14] M. A. Porras, A. Parola, D. Faccio, A. Dubietis, and P. Di Trapani, Nonlinear Unbalanced Bessel Beams: Stationary Conical Waves Supported by Nonlinear Losses, Phys. Rev. Lett. **93**, 153902 (2004).
[15] P. Johannisson, D. Anderson, M. Lisak, and M. Marklund, Nonlinear Bessel beams, Opt. Commun. **222**, 107 (2003).
[16] G. Xu, A. Mussot, A. Kudlinski, S. Trillo, F. Copie, and M. Conforti, Shock wave generation triggered by a weak background in optical fibers, Opt. Lett. **41**, 2656 (2016).
[17] M. A. Porras and F. Ramos, Quasi-ideal dynamics of vortex solitons embedded in flattop nonlinear Bessel beams, Opt. Lett. **42**, 3275 (2017).
[18] L. Zeng, J. Zeng, Y. V. Kartashov, and B. A. Malomed, Purely Kerr nonlinear model admitting flat-top solitons, Opt. Lett. **44**, 1206 (2019).
[19] S. Trillo and M. Conforti, in *Handbook of Optical Fibers*, edited by G. D. Peng (Springer, Singapore, 2017), pp. 1–48.
[20] D. Bongiovanni, B. Wetzel, P. Yang, Y. Hu, Y. Qiu, J. Xu, S. Wabnitz, Z. Chen, and R. Morandotti, Optical generation and control of spatial Riemann waves, Opt. Lett. **44**, 3542 (2019).
[21] S. Gentilini, N. Ghofraniha, E. DelRe, and C. Conti, Shock waves in thermal lensing, Phys. Rev. A **87**, 053811 (2013).
[22] Z. Chen, M. Mitchell, M. Shih, M. Segev, M. Garrett, and G. C. Valley, Steady-state dark photorefractive screening solitons, Opt. Lett. **21**, 629 (1996).